Rheophysics of dense granular materials: Discrete simulation of plane shear flows

Frédéric da Cruz, Sacha Emam, Michaël Prochnow, Jean-Noël Roux, and François Chevoir*
LMSGC, Institut Navier, 2 allée Kepler, 77 420 Champs sur Marne, France
(Received 22 February 2005; revised manuscript received 9 May 2005; published 31 August 2005)

We study the plane shear flow of a dense assembly of dissipative disks using discrete simulation and prescribing the pressure and the shear rate. Those shear states are steady and uniform, and become intermittent in the quasistatic regime. In the limit of rigid grains, the shear state is determined by a single dimensionless number, called the inertial number I, which describes the ratio of inertial to pressure forces. Small values of I correspond to the quasistatic critical state of soil mechanics, while large values of I correspond to the fully collisional regime of kinetic theory. When I increases in the intermediate dense flow regime, we measure an approximately linear decrease of the solid fraction from the maximum packing value, and an approximately linear increase of the effective friction coefficient from the static internal friction value. From those dilatancy and friction laws, we deduce the constitutive law for dense granular flows, with a plastic Coulomb term and a viscous Bagnold term. The mechanical characteristics of the grains (restitution, friction, and elasticity) have a small influence in the dense flow regime. Finally, we show that the evolution of the relative velocity fluctuations and of the contact force anisotropy as a function of I provides a simple explanation of the friction law.

DOI: 10.1103/PhysRevE.72.021309 PACS number(s): 45.70.Mg, 81.05.Rm, 83.10.−y, 83.80.Fg

I. INTRODUCTION

Due to their importance in geophysics and in various industrial processes, flows of granular materials are the focus of a large amount of research, at the frontier between physics and mechanics [1–3]. In order to predict propagation, flow rate, or jamming, one of the main objectives of these *rheophysical* studies is to determine the rheological laws, based on their physical origin at the scale of the grains and of their interactions. One thus tries to express the stress tensor (and especially the pressure P and the shear stress S, positively counted) as a function of the shear rate $\dot{\gamma}$ and other variables such as solid fraction ν. However, granular materials are extremely various, depending on the geometry of the grains and the nature of their interactions, and we restrict our attention to assemblies of cohesionless grains, slightly polydisperse, without interstitial fluid. This corresponds to macroscopic grains (diameter larger than 100 μm) in a fluid of low viscosity like air. The rheology is then only dictated by transfer of momentum and dissipation of energy taking place in direct contacts between grains and with the walls. Depending on the conditions, these materials reveal various mechanical behaviors, similar to those of elastoplastic solids in the quasistatic regime, to dense gases in the case of strong agitation, or to viscoplastic fluids when a flow is provoked. This paper is devoted to this intermediate *dense flow* regime, which is still not well understood. We first briefly recall the essential results for the two extreme regimes, quasistatic and collisional.

Dense, confined granular assemblies in extremely slow shear flow are usually described as solids abiding by elastoplastic, rate independent, constitutive laws [4–7]. After a large enough shear strain, the material reaches the *critical state* [8], which does not depend on its initial arrangement (loose or dense), and is characterized by an internal friction angle ϕ, defined as $\tan\phi = S/P$ in a simple shear test, by a critical solid fraction ν_c, and specific values for coordination number and distribution of contact orientations [9]. ϕ and ν_c depend only negligibly on the confining pressure P. In other words, the continuously sheared material can be modeled with the Coulomb criterion $S = P\tan\phi$, and in the following we shall discuss the effective friction coefficient $\mu^* = S/P$.

In the dilute limit and/or for strong agitation, the grains interact through binary, instantaneous, uncorrelated collisions. Then, the generalization of kinetic theory of dense gases to slightly dissipative grains [10–14] allows a hydrodynamical description. The stress components depend on the solid fraction and on the velocity fluctuations δv. In the two-dimensional geometry which we study in the following, the stress components are homogeneous to a force divided by a length. For an assembly of disks of diameter d and mass m,

$$P = F_P(\nu) m (\delta v/d)^2,$$

$$S = F_S(\nu) m (\delta v/d) \dot{\gamma}. \tag{1}$$

Solving a flow problem requires an additional equation of energy in which a dissipation rate Γ associated with dissipative collisions must be added to the usual terms:

$$\Gamma = F_\Gamma(\nu) m (\delta v/d)^3. \tag{2}$$

The dimensionless functions $F_i(\nu)$ are completely expressed as functions of the pair correlation function at contact $g_0(\nu)$. In the dense limit $(0.2 \leqslant \nu \leqslant 0.67)$, $F_i(\nu) \simeq A_i F(\nu)$, with $F(\nu) = \nu^2 g_0(\nu)$. In two dimensions, $g_0(\nu) = (16-7\nu)/16(1-\nu)^2$ [15]. The prefactors A_i are well-known functions of the restitution coefficient e [12]. In the case of a homogeneous shear flow, where the shear rate and the velocity fluctuations are uniform, the equation of energy reduces to a balance between the work of the shear stress and the dissipation:

*Corresponding author. Electronic address: chevoir@lcpc.fr

$S\dot{\gamma}=\Gamma$. This leads to $\delta v=\dot{\gamma}d\sqrt{A_S/A_\Gamma}$. Consequently, the stress components are equal to:

$$P = G_P(\nu)m\dot{\gamma}^2,$$

$$S = G_S(\nu)m\dot{\gamma}^2, \tag{3}$$

where $G_{P,S}(\nu)=B_{P,S}F(\nu)$ with $B_P=A_PA_S/A_\Gamma$ and $B_S=\sqrt{A_S^3/A_\Gamma}$. We notice that the effective friction coefficient is a constant ($\mu^*=\sqrt{A_SA_\Gamma/A_P^2}$), and that the solid fraction is a function of the dimensionless quantity $I=\dot{\gamma}\sqrt{m/P}$ [$\nu=G_P^{-1}(1/I^2)$]. This fully collisional description is relevant in the dilute limit when the inertial effects dominate.

In this paper, we focus our attention on the intermediate dense flow regime, where the solid fraction is close to a maximum solid fraction, so that the grains interact both through enduring contacts and through collisions. There is a contact network more or less percolating through the material and greatly fluctuating in space and time [16]. Such flows are beyond the quasistatic regime, since the inertia of the grains (and so the shear rate) certainly comes into play. On the other hand, the assumption of binary, instantaneous, uncorrelated collisions of kinetic theory is clearly in trouble. Due to the very strong correlations of motion and force, the theoretical description of those dense flows is very difficult and is still a matter of debate (see [17] for a recent review). Advances have come in the last decade from the combination of discrete numerical simulations and experiments on model materials in simple geometry, confined or free surface flows, and in various mechanical configurations. A detailed review of these works can be found in [18]. Depending on the mechanical configurations, the flows are steady, intermittent, or may even jam. A localization of the shear, with a width of a few grains, is also frequently observed near the walls or near the free surface, with exponential velocity profiles around. However, the heterogeneity of the stress distribution as well as the presence of walls makes the analysis of the constitutive law difficult.

This is the reason why we have chosen to study this dense flow regime in a steady homogeneous shear state (uniform stress components, shear rate, and solid fraction). We have studied the simplest geometry, plane shear without gravity, in which the stress distribution is uniform inside the shear layer. Furthermore, we have prescribed both the shear rate and the pressure. Using discrete numerical simulations, we have access to microscopic information, at the level of the grains and of the contact network, hardly measurable experimentally, and we are able to vary the parameters describing the grains and the shear state.

Due to its interest in rheology and more specifically in tribology (third body) and in geophysics (sliding of faults at the origin of earthquakes), this plane shear geometry has already been the subject of numerous discrete simulation studies [16,19–35].

Section II is devoted to the description of the simulated system. We show in Sec. III that we obtain steady uniform shear states in term of structure (solid fraction), kinematics (shear rate), and stress distribution. In Sec. IV, we discuss the dimensionless numbers that enter in the rheological laws, especially the inertial number I, which describes the shear state, and the contact stiffness number κ, which describes the typical deformation of the grains. In Sec. V, we measure the evolution of two macroscopic quantities (solid fraction and effective friction coefficient) as a function of I in the dense flow regime, from which we deduce the constitutive law. In Sec. VI from a parametric study, we show that this constitutive law is not very sensitive to the mechanical properties of the grains, once they are frictional, dissipative, and rigid. Then, we describe microscopic information on the fluctuations of the grain motion (Sec. VII) and on the contact network (Sec. VIII), from which we propose an explanation for the friction law (Sec. IX). For a more detailed account of the results, we refer to [36].

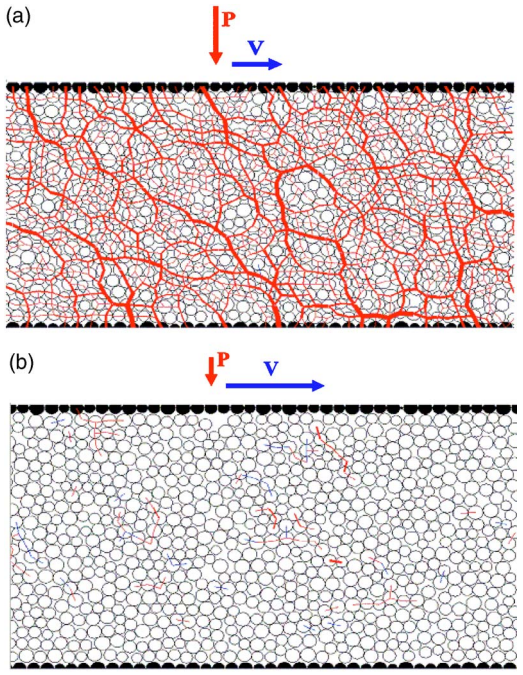

FIG. 1. (Color online) Plane shear: (a) quasistatic regime ($I=10^{-2}$); (b) collisional regime ($I=0.2$). (Black grains constitute the rough walls. The linewidths are proportional to the intensity of the normal force between grains.)

II. SIMULATED SYSTEM

The simulated system is two dimensional (Fig. 1). The granular material is a dense assembly of n dissipative disks of average diameter d and average mass m. A small polydispersity of ±20% is considered to prevent crystallization [15]. The mechanical properties of the grains are described by four independent parameters: a microscopic friction coefficient μ, a restitution coefficient in binary collisions e, and elastic stiffness coefficients k_n and k_t.

The granular material is submitted to a plane shear, without gravity, so that the stress distribution is uniform. The material is sheared between two parallel rough walls, distant from H. One of the walls is fixed, while the other moves at the prescribed velocity V. We call the flow direction x and the transverse direction y. Periodic boundary conditions are

TABLE I. List of system parameters.

n	L/d	H/d	$g_p/\sqrt{mk_n}$	I
900–5000	40–100	20–100	1	6×10^{-4}–0.3

TABLE II. List of material parameters.

Polydispersity	μ	e	k_t/k_n	κ
±20%	0–0.8	0.1–0.9	0.5	$40-2.5\times10^5$

applied along the flow direction, and we call the length of the simulation box L (always larger than 40 grains). The wall roughness is made of contiguous grains sharing the characteristics of the flowing grains (same polydispersity and mechanical properties—no rotation). $y=0$ corresponds to the center of the glued grains on the fixed wall.

An important feature of our simulation is that we chose to control the lateral pressure Σ_{yy} rather than keeping the solid fraction fixed, which is appropriate to discuss real flows since experimental conditions usually determine stress levels, rather than solid fraction. We shall see in the following that the normal stress components Σ_{xx} and Σ_{yy} are equal, so that Σ_{yy} is equal to the pressure $P=(\Sigma_{xx}+\Sigma_{yy})/2$. The control of the pressure P is achieved by allowing the dilatancy of the shear cell along y (H is not fixed), through the vertical motion of the moving wall given by $\dot{H}=(P-P_w)L/g_p$, where g_p is a viscous damping parameter, and P_w is the normal stress exerted by the grains on the moving wall. Steady state corresponds to $\langle P_w\rangle=P$.

The parameters of the simulated system are summarized in Table I (anticipating Sec. IV, we indicate the values of the dimensionless parameters $g_p/\sqrt{mk_n}$ and I).

Let us consider two grains i and j in contact, of diameter $d_{i,j}$, mass $m_{i,j}$, centered at position $\vec{r}_{i,j}$, with velocity $\vec{v}_{i,j}$ and rotation rate $\omega_{i,j}$. Let $\vec{n}_{ij}$ denote the normal unit vector, pointing from i to j ($\vec{n}_{ij}=\vec{r}_{ij}/\|\vec{r}_{ij}\|$ with the notation $\vec{r}_{ij}=\vec{r}_j-\vec{r}_i$), and $\vec{t}_{ij}$ a unit tangential vector such that $(\vec{n}_{ij},\vec{t}_{ij})$ is positively oriented. We denote by $\vec{F}_{ij}=N_{ij}\vec{n}_{ij}+T_{ij}\vec{t}_{ij}$ the contact force exerted on the grain j by the grain i. The *contact law* relates the normal, N_{ij}, and tangential, T_{ij}, components of the contact force to the corresponding components of relative displacements and/or velocities. The relative velocity at the contact point is equal to $\vec{V}_{ij}=\vec{v}_i-\vec{v}_j+1/2(d_i\omega_i+d_j\omega_j)\vec{t}_{ij}$. Its normal component $V_{ij}^N=\vec{n}_{ij}\cdot\vec{V}_{ij}$ is the time derivative of the normal deflection of the contact (or apparent "interpenetration" of undeformed disks), $h_{ij}=(d_i+d_j)/2-\|\vec{r}_{ij}\|$. Its tangential component $V_{ij}^T=\vec{t}_{ij}\cdot\vec{V}_{ij}$ is the time derivative of the tangential relative displacement δ_{ij}.

The normal contact force is the sum of two contributions, an elastic one N^e and a viscous one N^v: $N_{ij}=N_{ij}^e+N_{ij}^v$. Keeping in mind that contacts have to close to transmit forces ($\vec{F}_{ij}=\vec{0}$ if $h_{ij}\leqslant0$) the linear (unilateral) elastic law reads $N_{ij}^e=k_nh_{ij}$, which involves a constant normal stiffness coefficient k_n, the value of which is independent of the disk radii. Physically, this can be regarded as a simplified version of the Hertz law [37], $N^e\propto h^{3/2}$. The normal viscous force opposes the relative approaching or receding velocity $N_{ij}^v=\zeta_{ij}\dot{h}_{ij}$, where ζ_{ij} is related to the normal restitution coefficient e in a binary collision, and chosen such that e is constant for all contacting pairs, whence $\zeta_{ij}=\sqrt{m_{ij}k_n}(-2\ln e)/\sqrt{\pi^2+\ln^2 e}$, where $m_{ij}=m_im_j/(m_i+m_j)$. The viscous dissipation might stem from the viscoelasticity of the grain material [38]. The total normal force might be either repulsive or attractive, due to the viscous contribution. We can check that setting N_{ij} to zero whenever it becomes attractive ($N_{ij}\leqslant0$) has but a negligible effect on the simulation results [39].

The Coulomb condition in the contacts involves the microscopic coefficient of friction between grains μ, and is enforced with the sole elastic part of the normal force $|T_{ij}|\leqslant\mu N_{ij}^e$. To this end, the tangential component of the contact force is related to the *elastic part* δ_{ij}^e of the relative tangential displacement δ_{ij}, $T_{ij}=k_t\delta_{ij}^e$, with a tangential stiffness coefficient k_t. δ_{ij}^e is defined by $d\delta_{ij}^e/dt=0$ if $|T_{ij}|=\mu N_{ij}^e$ and $T_{ij}V_{ij}^T\geqslant0$ and $d\delta_{ij}^e/dt=V_{ij}^T$ otherwise. The contact is termed "sliding" in the first case and "rolling" in the second case.

Table II gives the list of material parameters (anticipating Sec. IV, we indicate the value of the dimensionless parameter κ).

The interaction law being chosen, numerical simulations are carried out with the molecular dynamics method, as in Refs. [40–42]. The equations of motion are discretized using a standard procedure (Gear's order 3 predictor-corrector algorithm [43]). The time step is a small fraction (1/100) of the duration τ_c of a binary collision between two grains of mass m [$\tau_c=\sqrt{m(\pi^2+\ln^2 e)/(4k_n)}$].

III. STEADY UNIFORM SHEAR STATE

Two kinds of preparation have been compared. The first kind (which has been used most of the time) consists in starting from an initial configuration where the disks are randomly deposited without contact and at rest between the two distant walls, which provides an average solid fraction of 0.5, and then in applying the pressure to the wall while slowly shearing the granular material. When the pressure on the walls reaches the prescribed value, the prescribed velocity is applied. The second kind consists in starting from a very high solid fraction (of the order of 0.8), obtained by a random deposit followed by a cyclic compaction with frictionless grains, and then introducing friction between grains and starting the shear with the prescribed velocity and pressure. The two kinds of preparation allow one to start either from a loose state (the first case), or from a dense state (the second case). Occasionally, we have used a third kind of preparation consisting in starting from localized shear states near one of the walls (obtained by applying gravity [36]).

We then look for a steady flow, characterized by constant time-averaged quantities of the flowing layer, like kinetic energy and solid fraction. We have observed that, after a sufficient amount of time, the three kinds of preparation lead to the same shear state. We deduce that there is no influence of the preparation on the steady flow characteristics. All the simulations converge to an average steady state. We consider

that the shear state is continuous if the relative fluctuations of the measured quantities are small enough (for instance the H fluctuations remain smaller than 1% [36]), otherwise the flow is called intermittent (see Sec. VII A). When a steady state is reached, the simulation is carried on during a sufficient amount of time Δt, so that the typical relative displacement of two neighboring layers is larger than ten grains ($\dot{\gamma}\Delta t \geqslant 10$). In this steady state, we consider that the statistical distribution of the quantities of interest (structure, velocities, forces, etc.) are independent of t and x, so that we average both in space (along x) and in time (considering 200 time steps distributed over the period Δt).

Using averaging methods described in [44,45], we measure the profiles of solid fraction, shear rate, and the components of the stress tensor [36]. The stress tensor $\underline{\underline{\Sigma}}$ is the sum of two contributions [46,47]:

$$\underline{\underline{\Sigma}} = \underline{\underline{\Sigma}}^c + \underline{\underline{\Sigma}}^f. \tag{4}$$

The first term ("contact"), usual in statics of granular materials, is associated with contact forces between grains [48,49]. The second term ("fluctuations"), usual in fluid mechanics (Reynolds tensor), is associated with the velocity fluctuations of the grains $\delta\vec{v}_i$:

$$\underline{\underline{\Sigma}}^c = \frac{1}{LH}\sum_{i\leqslant j} \vec{F}^{ij} \otimes \vec{r}^{ij},$$

$$\underline{\underline{\Sigma}}^f = \frac{1}{LH}\sum_{i=1}^{n} m_i \delta\vec{v}_i \otimes \delta\vec{v}_i. \tag{5}$$

A third contribution, associated with the rotation of the grains [50], is very small. In the dense flow regime, the stress tensor is dominated by the contact term [36].

We observe that, apart from the five first layers near the walls, the granular material is homogeneously sheared: the solid fraction, shear rate, and stress components are approximately constant in the central part of the sheared layer. Consequently, all the averaged quantities are measured in the central part of the sheared layer, excluding the five first layers near the walls, and H is chosen large enough so as to limit those wall effects [we have also tested the homogeneity of the shear in the case of a thin layer ($H/d \approx 5$) [36]].

This absence of localization is in contrast with other studies [19,27,29,30]. However, we have observed signs of localization in the quasistatic regime where the flow becomes intermittent (Sec. VII), and in the case of a very small polydispersity ($\leqslant 1\%$), where the granular material crystallizes near the walls and the shear zone reduces to a ten diameter thick central layer [36].

We observe that $\Sigma_{xx} \simeq \Sigma_{yy}$ (within less than 5%). This has also been observed in other shear geometries (inclined planes, annular shear) and with other discrete simulation methods [35,36,41,45]. This observation is in contrast with the usual Mohr-Coulomb behavior in soil mechanics, where the ratio of Σ_{xx} and Σ_{yy} is equal to an active or passive Rankine coefficient, different from unity [5]. In discrete simulation of biaxial tests, it has been recently observed that this ratio tends to unity when reaching the critical state [51]. Consequently the pressure $P=(\Sigma_{xx}+\Sigma_{yy})/2 \simeq \Sigma_{yy}$. In the following we set $S=-\Sigma_{xy}$.

IV. DIMENSIONLESS NUMBERS

A. Dimensional analysis

In our discrete numerical simulations, the physical system is completely described by a list of independent parameters associated with the grains and with the shear state. The grains are described by their size d, mass m, coefficient of restitution e, coefficient of friction μ, and elastic stiffness parameters k_n and k_t. k_t is of the same order of magnitude as k_n [37], and as it has a very small influence on the results [31,41], it was fixed to $k_n/2$ in all our calculations. The shear state is described by the prescribed pressure P, the velocity V, the height H, and the viscous damping parameter g_p. As we study the dense granular flow in the uniform sheared layer at distance from the walls, we consider the shear rate $\dot{\gamma}$, rather than V and H separately. We have not studied the influence of the normal motion of the wall controlling the pressure, described by the dimensionless number $g_p/\sqrt{mk_n}$. With the value of 1 chosen in all our simulations, we consider that the time scale of the fluctuations of H is imposed by the material rather than the wall, and that the wall "glues" to the material. Close to the quasistatic regime, its influence may be important, but we notice that in the dense flow regime, the profiles obtained for controlled pressure are in agreement with the one measured at fixed volume [52]. Consequently, the shear state is described by the pressure P and the shear rate $\dot{\gamma}$.

As a way to reduce the number of parameters, it is convenient to use dimensional analysis, which guarantees that all the results can be expressed as relations between dimensionless quantities. There are already two dimensionless quantities e and μ. Apart from the length and mass scales d and m, there remain three dimensional quantities P, $\dot{\gamma}$, and k_n, from which we can build two dimensionless numbers. Among the various possible choices, we propose to use the following pair:

$$\kappa = \frac{k_n}{P},$$

$$I = \dot{\gamma}\sqrt{\frac{m}{P}}. \tag{6}$$

All measured dimensionless quantities (solid fraction ν, effective friction coefficient μ^*, relative velocity fluctuations, coordination number, mobilization of friction, etc.) will hereafter be given as functions of I and κ.

We now provide a physical interpretation of those two dimensionless numbers, by considering them as dimensionless ratios of typical quantities in the system, such as time scales: the collision time τ_c (which is comparable to the propagation time of the impulse through a grain), the shear time $\tau_s = 1/\dot{\gamma}$, and the inertial time $\tau_i = \sqrt{m/P}$ (the characteristic displacement time of a grain of mass m submitted to a pressure P).

B. Contact stiffness number

κ is proportional to the ratio of time scales $(\tau_i/\tau_c)^2$. More simply, it is the ratio of the stress scales k_n and P, and is inversely proportional to the normal deflection h/d of the contacts for a confining pressure P. Consequently, it may be called the *contact stiffness number*. A large value corresponds to rigid grains, while a small value corresponds to soft grains.

From previous numerical studies on quasistatic deformation [53], it is known that contact stiffness parameters have a negligible influence on macroscopic mechanical properties at moderate or large strains when κ exceeds 10^4, which we call the *rigid grain limit*. Then the elastic deformations stay negligible in comparison with the gaps between neighboring grain surfaces that determine the amplitude of rearrangement events (a more stringent condition than $h \ll d$). As a way to give an estimate for κ in a realistic problem, we consider a layer of glass beads submitted to its own weight. This cannot be directly compared with the simulated system where there is no gravity. However, the weight of the layer (50 cm thick) provides a typical scale of pressure ($P=10$ kPa). For Hertzian contacts, an appropriate definition of κ, such that typical contact deflections satisfy $h/d \propto \kappa^{-1}$ with a coefficient of order 1, is $\kappa=(E/P)^{2/3}$, with E the Young modulus [37]. Considering glass beads ($E=70$ GPa) under $P=10$ kPa, this yields $\kappa \simeq 37\,000$. This example shows that usual situations are very close to the rigid grain limit studied in this paper.

C. Inertial number

As the ratio of inertial to shear times or equivalently the ratio of inertial forces to confining forces, I measures the inertial effects, and will be called the *inertial number* in the following. A small value of I (small $\dot{\gamma}$ and/or large P) corresponds to a regime where the grain inertia is not relevant: this is the quasistatic critical state regime [Fig. 1(a)]. Inversely, a large value of I (small P and/or large $\dot{\gamma}$) corresponds to the collisional regime, which may be described by kinetic theory [Fig. 1(b)]. Varying I allows one to study the progressive transition between those two regimes. We notice that it already appeared in the collisional regime (Sec. I), and that it is a variant (square root) of the previously defined *Savage number* [54] and *Coulomb number* [55]. Using the mass density ρ_g of the grains, it may also be written $I=\dot{\gamma}d\sqrt{\rho_g/P}$.

I describes the shear state, through a combination of the shear rate and pressure. When varying independently the shear rate (factor F) and the pressure (factor F^2) while keeping the same value of I, the two flow configurations will be the same. We have studied various systems with different shear rate and pressure but the same inertial number (for instance for $H/d=20$, $V=1-P=25$ and $V=0.1-P=0.25$, factor $F=10$), and we have not measured any difference in the macroscopic quantities. The data shown on the forthcoming figures of the paper correspond to such cases. If we vary k_n (factor F^2) in such a way that κ is unchanged, there is no difference at all, since this is the same simulation: τ_c and hence the time step is modified (factor $1/F$), so that the deformation of the system in one time step remains exactly the same. If we let κ vary according to the variation of P (factor $1/F^2$), small variations may be observed on the coordination number, or when the system leaves the rigid grain limit.

D. Comments

Some authors [20,31] chose to control the solid fraction ν rather than the pressure, and therefore, rather than I and κ, used the pair of dimensionless numbers ν and $\alpha=\dot{\gamma}/\sqrt{k_n/m}=I/\sqrt{\kappa}$ as variables characterizing the state of the granular material in steady uniform shear flow. α may be viewed as the ratio of the collision time to the shearing time, or as the shearing velocity divided by the sound velocity (Mach number [31]). Both choices are perfectly legitimate, as dimensional analysis predicts either $\mu^*=f_1(I,\kappa)$ and $\nu=f_2(I,\kappa)$, or $\mu^*=f_3(\nu,\alpha)$ and $\kappa=f_4(\nu,\alpha)$, both results being equally valid. The choice of I and κ can, however, be deemed more convenient for several reasons. First, the variation of the results with ν, regarded as a control parameter, is extremely fast. Each material possesses a critical packing fraction ν_c, in the sense of Sec. I, above which it does not flow, unless stresses are so large that the elastic compression of contacts compensates for the difference $\nu-\nu_c$. Below ν_c, on the other hand, a continuously sheared granular system is free to flow with a negligible shear stress, unless the velocity is high enough to build a significant pressure. One should therefore monitor ν with great accuracy to observe ordinary stress levels. This renders the comparisons between different granular systems difficult, as one would need to know in advance the value of the critical density for each of them. Furthermore, the limit of rigid grains becomes singular, as all values of ν above ν_c are strictly forbidden for $\dot{\gamma} \neq 0$, while all the properties of shear flows with $\nu \leqslant \nu_c$ scale as a power of $\dot{\gamma}$ in that limit [35]. Hence, no change of flow regime is expected on changing $\dot{\gamma}$, which appears to contradict intuition unless one recalls that the rigid grain limit, on increasing flow rates, will eventually require unreasonably large contact stiffnesses, due to very high pressure levels. Conversely, if one uses I and κ as control parameters, no singularity enters any of the relevant results in the $I \to 0$ or $\kappa \to \infty$ limits, and different materials should exhibit similar (if not quantitatively identical) behaviors for the same values of these parameters (which thus define roughly "corresponding states").

V. CONSTITUTIVE LAW

We are going to show that the inertial number is a fundamental quantity to describe the rheology of granular materials, as previously anticipated in [54,55]. In the steady uniform shear states, the solid fraction and the shear stress adjust in response to the prescribed inertial number. In this section, we now show the strong influence of I on two dimensionless quantities, the solid fraction and the effective friction coefficient. We defer the detailed discussion of the influence of the various mechanical parameters of the grains (κ, e, and μ) to the next section. If not specified otherwise, we have chosen the following values of the parameters: $\kappa=10^4$, $e=0.1$, and $\mu=0.4$.

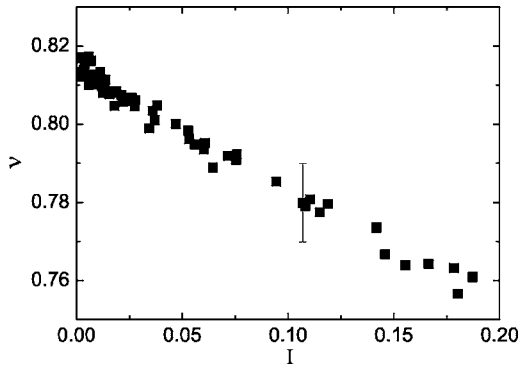

FIG. 2. Dilatancy law (μ=0.4, various e and κ).

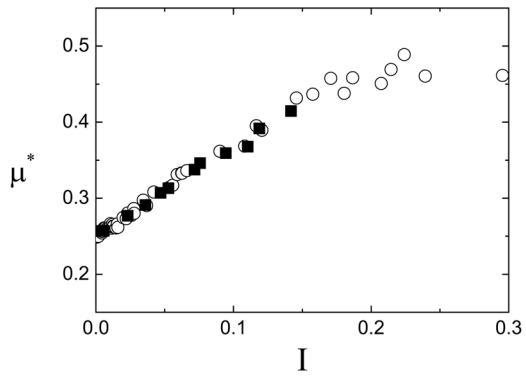

FIG. 3. Friction law (μ=0.4, e=0.1 (○), e=0.9 (■), various κ).

A. Dilatancy law

We call the variations of the average solid fraction ν as a function of the inertial number I the dilatancy law (Fig. 2). We observe that ν decreases approximately linearly with increasing I, starting from a maximum value ν_{max}:

$$\nu(I) \simeq \nu_{max} - aI, \tag{7}$$

with $\nu_{max} \simeq 0.81$ and $a \simeq 0.3$ (for μ=0.4). The error bar (independent of I) corresponds to the statistical dispersion inside the layer. This averaged measurement can be complemented by the measurement of the spatial heterogeneity (distribution of local solid fraction) within the sheared layer, which increases with I [56].

B. Friction law

The effective friction coefficient has been defined as the ratio of the shear stress to the pressure inside the material $\mu^* = S/P$. It could also be defined as the ratio of the (total) tangential and normal forces on the wall $\mu_w^* = T/N$. We have observed [36] that μ_w^* is slightly larger than μ^*. Some simulations have been carried out to test the influence of the roughness, by taking glued grain on the wall twice as small (R=0.5) or twice as large (R=2) as the flowing grains, for the same I_g. This size ratio has an influence on the sliding velocity at the wall: it becomes noticeable for R=0.5 and decreases when R increases, since the grains close to the walls are trapped by the roughness. However, at a distance from the walls, the flow remains uniform, but the shear rate, and hence I, decreases when R decreases. Furthermore, the effective friction at the wall decreases when R decreases. All in all, $\mu_w^*(I)$ seems independent of R. For a more detailed discussion of the influence of the roughness on the flow (inclined plane and vertical chute), we refer to [18,45,57]. In the following we shall only discuss the effective friction coefficient in the volume of the flowing layer.

We call the variations of the effective friction coefficient μ^* (averaged over the width in the central part of the flowing layer) as a function of I the friction law (Fig. 3). We observe that μ^* increases approximately linearly with I, starting from a minimum value μ_{min}^*:

$$\mu^* \simeq \mu_{min}^* + bI, \tag{8}$$

with $\mu_{min}^* \simeq 0.25$ and $b \simeq 1.1$ (for μ=0.4), and saturates for $I \geqslant 0.2$. The error bars (independent of I) correspond to the statistical dispersion inside the layer. We also observe that μ^* tends to saturate for $I \geqslant 0.2$. Within the error bars, it is difficult to be more precise about those dependencies. A more careful measurement is deferred for future work.

We now compare this friction law with other works. We first notice that the increase of μ^* with I is contrary to the well-documented decrease of the friction coefficient with the velocity in the quasistatic regime [58]. However, in those studies, this softening is interpreted as a consequence of the renewal of the population of asperities at a microscopic scale, or as an effect of humidity [59]. Those effects do not come into play in our study. As a matter of fact, this friction law was already observed in previous discrete simulations [23], and partial observations (experimental or numerical) of the variation of μ^* with the shear rate, the pressure or the solid fraction, consistent with our observations, may be found in [21,27,59–64]. Interestingly, the inclined plane geometry allows one to prescribe both the effective friction and the pressure, through the inclination θ of the plane and the height H of the flowing layer. Consequently, the measure of the superficial velocity V as a function of these two parameters provides a measure of the friction coefficient at the base as a function of I_g (which is proportional to $V/H^{3/2}$) [65,66]. Those observations are in good agreement with the previous friction law [36,67].

C. Comments

The classification of the flow regimes strongly depends on the single dimensionless number I. In the quasistatic regime ($I \leqslant 10^{-2}$), the granular material is very dense, close to the maximum solid fraction ν_{max}, and the effective friction coefficient is close to its minimum value μ_{min}^*. In the collisional regime ($I \geqslant 0.2$), the dilatancy becomes strong and the effective friction coefficient seems to saturate. The transition between those two regimes is progressive. In the dense flow regime ($10^{-2} \leqslant I \leqslant 0.2$), we observe approximately linear variations of the solid fraction and of the effective friction coefficient as a function of I [Eqs. (7) and (8)]. The dilatancy

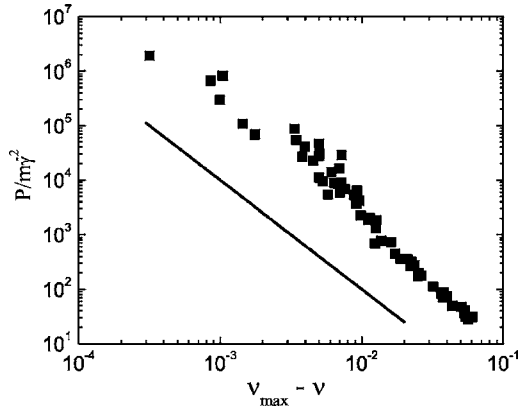

FIG. 4. $P/\dot{\gamma}^2$ as a function of $(\nu_{max}-\nu)$. The straight line indicates a slope of -2 ($\mu=0.4$, various e).

and friction laws, measured in the whole range of regimes, from the quasistatic to the collisional, make the link between the known results in the two extreme regimes recalled in Sec. I. In the quasistatic regime, μ_{min}^* and ν_{max} may be identified with the internal friction tan ϕ and the critical solid fraction ν_c in the critical state.

When taking into account the elasticity of the grains, it is natural to draw a diagram of the flow regimes as a function of the two dimensionless numbers $\alpha=I/\sqrt{\kappa}$ and ν [20,31]. This leads us to identify three regimes: elastic quasistatic, purely inertial, and elastic inertial. This last regime corresponds to very soft grains ($\kappa\leqslant 100$) and is not accessible in our study, where we stay in the limit of rigid grains. Furthermore, various studies where the volume rather than the pressure was prescribed [20,26,31,68] have evidenced a transition between the quasistatic and the inertial regimes around a critical solid fraction. In our study where the pressure is prescribed, the solid fraction adjusts to the inertial number I, so that the transition is not accessible.

D. Constitutive law

These dilatancy and friction laws allow us to deduce the dependencies of the pressure and shear stress on the shear rate and solid fraction: $P(\nu,\dot{\gamma})$ and $S(\nu,\dot{\gamma})$.

From the definition of I [Eq. (6)] and the dilatancy law [Eq. (7)], the pressure may be expressed as a function of the shear rate and the solid fraction:

$$P(\nu,\dot{\gamma})=\frac{a^2}{(\nu_{max}-\nu)^2}m\dot{\gamma}^2. \tag{9}$$

The divergency with the solid fraction is shown in Fig. 4.

From the definition of I [Eq. (6)] and the friction law [Eq. (8)], the shear stress may be expressed as a function of the shear rate and the pressure:

$$S(P,\dot{\gamma})=\mu_{min}^*P+b\sqrt{mP}\,\dot{\gamma}. \tag{10}$$

Using the previous expression of P [Eq. (9)], it is also possible to express the shear stress as a function of the shear rate and the solid fraction:

$$S(P,\nu,\dot{\gamma})=\mu_{min}^*P+\frac{ab}{(\nu_{max}-\nu)}m\dot{\gamma}^2, \tag{11}$$

or, eliminating P,

$$S(\nu,\dot{\gamma})=\frac{ab(\nu^*-\nu)}{(\nu_{max}-\nu)^2}m\dot{\gamma}^2, \tag{12}$$

with the solid fraction $\nu^*=\nu_{max}+a\mu_{min}^*/b$ ($\nu^*\approx 0.86$ for $\mu=0.4$).

For $I\leqslant 0.2$, the expression of the stress components is analogous to the expression for a steady uniform system in the fully collisional regime [Eqs. (3)]. The dependence on the square of the shear rate, similar to the original conclusions of Bagnold for concentrated suspensions [69], is a consequence of dimensional analysis [35]. The dependencies on solid fraction are described by the following dimensionless functions:

$$G_P(\nu)=\frac{a^2}{(\nu_{max}-\nu)^2},$$

$$G_S(\nu)=\frac{ab(\nu^*-\nu)}{(\nu_{max}-\nu)^2}. \tag{13}$$

We recall that kinetic theory predicts a divergency in $1/(1-\nu)^2$ from the asymptotic behavior of the pair correlation function (see Sec. I). However, when $\nu\geqslant 0.67$ (so-called gel transition), then starts a regime of multiple collisions, strongly correlated, and the divergency rather seems in $1/(\nu_{max}-\nu)$ [15,32]. When the material is sheared, under the effect of cooperative rearrangements of caged grains, an even stronger divergency of the viscosity has been conjectured [70]. The precise form of these divergencies is decisive to describe the shape of the velocity profiles and for the jamming process [70–72]. Our quantitative determination is then precious information for the modeling of dense granular flows.

We also notice that the expression (10) of S corresponds to a viscoplastic constitutive law, similar to the "frictional-collisional" decomposition of the stress tensor, with a contribution associated to maintained contacts, and a contribution associated with collisions [32,72–78]. In the viscous term, we notice that the apparent viscosity $b\sqrt{mP}$ is proportional to the square root of the pressure. The interpretation is that the typical momentum $m\dot{\gamma}d$ is exchanged with the inertial time scale $\sqrt{m/P}$ over a surface of the order d^2.

We think that the formulation of the constitutive law through the dilatancy and friction laws is simpler to use, since it avoids the treatment of divergency near jamming, which might be a problem in fluid mechanical numerical simulations.

VI. INFLUENCE OF THE MECHANICAL PARAMETERS

We now describe the influence of the mechanical properties of the grains on the constitutive law. e has been varied between 0.1 and 0.9, μ between 0 and 0.8, and κ between 40 and 2.5×10^5. We show that the constitutive law is not sensitive to κ once the grains are rigid enough ($\kappa\geqslant 10^3$), nor to

e once the grains are frictional, which is the usual situation in practice. However, it is sensitive to μ, and to e for $\mu=0$, and $I \geqslant 0.1$.

A. Influence of the elasticity of the grains

We have observed that there is no influence of κ on the constitutive law once it is larger than 10^4 (or even 10^3), except on the coordination number (see Sec. VIII A). However, for small values (40), we have observed a localization of the shear near the moving wall in a large system ($H/d=100$) [36], which we interpret as an effect of the decrease of the correlation length of the strain field when the grains become softer. We notice that $\kappa=10^4$ corresponds to $\tau_i/\tau_c=10^2$. Since $I=\tau_i/\tau_s$ is smaller than around 0.1 in the dense flow regime, τ_s is at least 1000 times larger than τ_c in the rigid grain limit [78]. Consequently, we may speak of a rigid grain limit in the dense flow regime, and our results should be comparable to the ones obtained with rigid grains simulation methods [35].

B. Influence of the microscopic friction coefficient

The microscopic friction coefficient μ has a significant influence on the dilatancy law. The solid fraction remains a linearly decreasing function of I, but both parameters ν_{max} and a depend on μ.

The variation of a is not simple: we measure $a=0.38$ for $\mu=0,0.31$ for $\mu=0.4$, and 0.37 for $\mu=0.8$ [36]. Figure 5(a) indicates that ν_{max} is a decreasing function of μ (it is not purely geometrical in the quasistatic regime). This shows that the solid fraction, from the critical state to the collisional regime, depends on the frictional properties of the material, in agreement with other observations [26,31].

The influence of μ on the friction law is less significant, except for frictionless grains ($\mu=0$), as shown in Fig. 6, where μ varies between 0 and 0.8. This variation is more significant for small I. Figure 5(b) shows more precisely the variation of the effective friction as a function of μ in the quasistatic regime. There is strong variation between $\mu=0$ and 0.4, but above $\mu=0.4$ the effective friction remains constant.

As a conclusion, in the case of frictionless grains, the friction law keeps the same tendency but is shifted toward smaller values of friction (Fig. 6). However, we observe a saturation for $I \geqslant 0.1$ if $e=0.9$, which will be discussed in Sec. VI D. For $I \leqslant 0.1$, the linear approximation [Eq. (8)] is in trouble: it is rather a sublinear dependency, and $\mu^*_{min} \simeq 0.11$.

Starting from both variations of solid fraction and effective friction as a function of the local friction coefficient μ, it is tempting to draw the variations of the effective friction as a function of solid fraction instead of inertial number. This is done on Fig. 7. As a matter of fact, Eqs. (9) and (12) predict

$$\mu^*(\nu) = \frac{b}{a}(\nu^* - \nu), \tag{14}$$

where ν^* was previously defined. This representation of the results evidences a collapse of the data (even if a, b, μ^*_{min}, and ν_{max} vary separately with μ, $\nu^* = \nu_{max} + a\mu^*_{min}/b$ seems approximately constant). It appears that μ^* becomes nearly independent of μ. This master curve is made of complementary zones of high solid fraction for frictionless grains and smaller solid fraction for frictional grains, and is of help in rheological models [72]. It is noteworthy that a variation of solid fraction of the order of 10% is enough to induce a variation of effective friction by a factor 4. This decrease of the effective friction when the solid fraction increases was previously observed under shear [62].

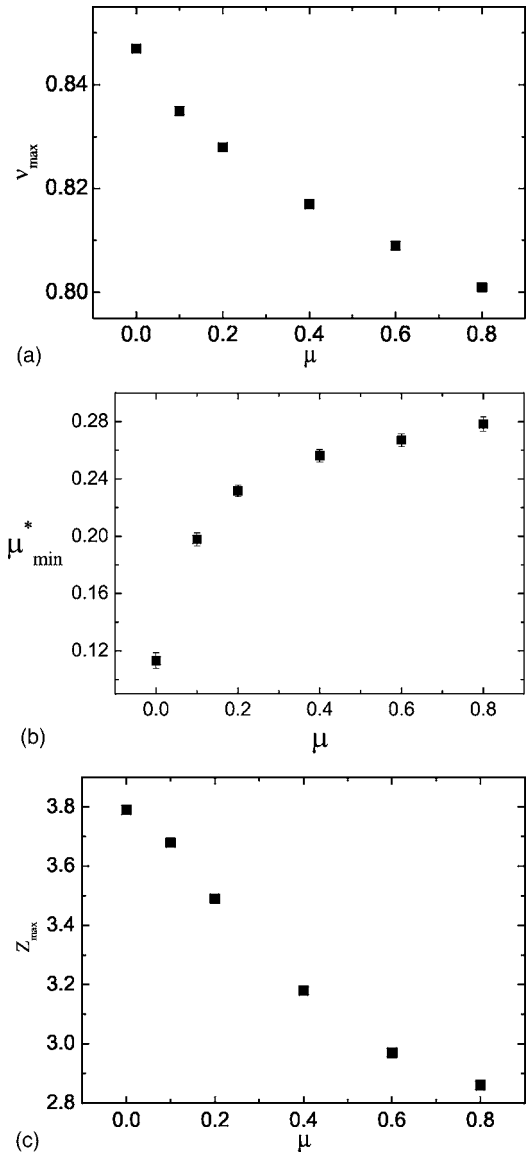

FIG. 5. Influence of μ on the critical state ($I=4\times10^{-3}$ and $e=0.1$): (a) maximum packing fraction ν_{max}, (b) effective friction coefficient μ^*_{min}, and (c) coordination number Z_{max}.

C. Influence of the restitution coefficient

Figure 3 shows that there is no influence of the restitution coefficient e for $\mu=0.4$. For frictionless grains, the comparison between slightly ($e=0.1$) and strongly ($e=0.9$) dissipative grains reveals (Fig. 8) that there is an influence, limited

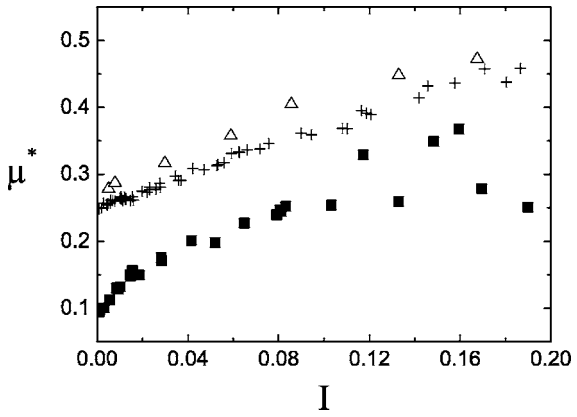

FIG. 6. Influence of μ on the friction law: (μ=0 (■), μ=0.4 (+), μ=0.8(△), various e.

to the collisional regime, for $I \geqslant 0.1$. Then, as the dissipation decreases, the dilatancy is less pronounced and the effective friction saturates (see also [31]).

D. Collisional limit

The situation ($I \geqslant 0.1$, μ=0, and e=0.9) corresponds to the dense limit of kinetic theory, with binary slightly dissipative collisions (then the average contact time tends to the collision time [52]). In this dense limit, Eqs. (3) predict a value of the effective friction independent of I but dependent on e, from the values of the prefactors A_i [12]:

$$\mu^*(e) = \frac{\sqrt{A_S A_\Gamma}}{A_P} = \frac{1}{2}\left(\frac{\pi+8}{2\pi}\right)^{1/2}\sqrt{1-e^2}. \qquad (15)$$

For e=0.9, this predicts μ^*=0.29 which is in fairly good agreement with the value measured for I=0.2 (0.26). The small difference between those two values may be due to the influence of the walls which induce a sliding velocity and gradients of the fluctuations [79].

VII. FLUCTUATIONS

Up to now, all the quantities (solid fraction, velocities, forces) have been averaged in space and time. In fact, they

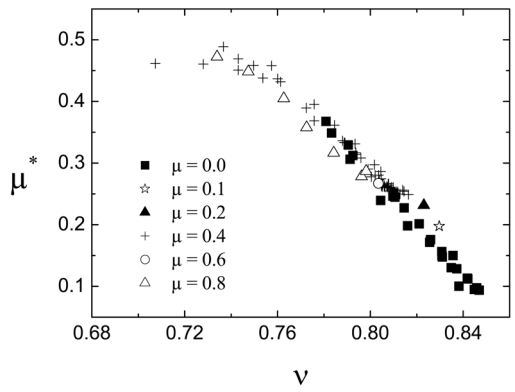

FIG. 7. Variation of the effective friction coefficient as a function of solid fraction.

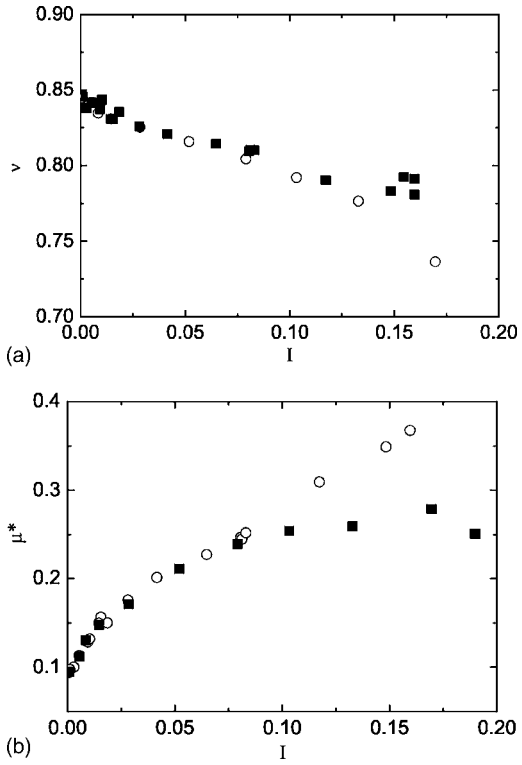

FIG. 8. Influence of e for μ=0 [e=0.9 (■), e=0.1 (○): (a) dilatancy law; (b) friction law.

are heterogeneous in space and fluctuate in time. We now discuss the fluctuations of the motion of the grains.

A. Intermittencies in the quasistatic regime

Various studies have shown that granular flows become unstable in the quasistatic regime. When the velocity is prescribed, one goes from a continuous flow regime to stick-slip [59,80,81]. When the shear stress is prescribed, one observes a hysteretic and abrupt fluid-solid transition [82]. The observation of shear localization in discrete simulations of plane shear corresponds to the quasistatic regime [27,30]. Our study shows that the flow is continuous in the dense flow regime, but becomes intermittent in the quasistatic regime (for $I \leqslant I_0 \simeq 0.003$). Then the time-averaged quantities are uniform, but the layer oscillates between two localized states near the moving or the fixed wall. Those two extreme states have a very short duration, and the system is most of the time in an intermediate state, where the shear is approximately uniform in the whole layer. Consequently, the total kinetic energy fluctuates in time, with sudden peaks associated to the two extremal states, and slow variations associated with the intermediate situations. Figure 9 indicates that the relative fluctuations of the kinetic energy increase when I decreases and saturate in the quasistatic regime, according to

$$\frac{\Delta E_c}{\langle E_c \rangle} \simeq \begin{cases} \dfrac{c}{I_0} & \text{for } I \leqslant I_0, \\ \dfrac{c}{I} & \text{for } I \geqslant I_0, \end{cases} \qquad (16)$$

with $I_0 \simeq 0.003$.

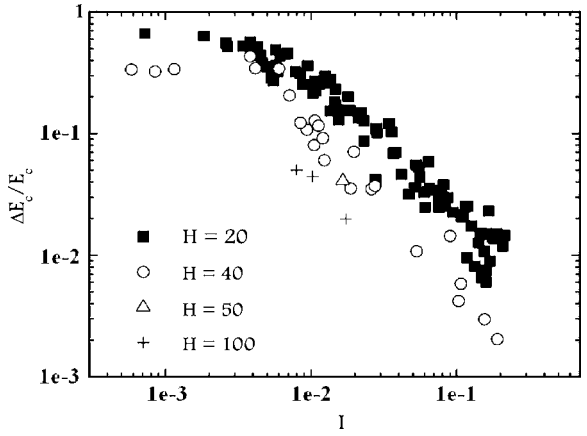

FIG. 9. Relative fluctuations of the kinetic energy as a function of I. Influence of H.

B. Velocity fluctuations

We now discuss the fluctuations of the translation velocity δv and of the rotation velocity $\delta\omega$ of the grains (measured in the central part of the sheared layer, excluding the five first layers near the walls). They are defined by

$$\delta v = \sqrt{\langle \vec{v}^2 \rangle - \langle \vec{v} \rangle^2},$$

$$\delta\omega = \sqrt{\langle \omega^2 \rangle - \langle \omega \rangle^2}. \tag{17}$$

Their influence is difficult to analyze in dense flows, where the motions of the grains are strongly correlated [35]. Their definition is a problem, since it has been shown that they depend on the averaging time scale [16]. Our analysis (long time scale) takes into account both the small fluctuations around the mean motion (in the "cage" formed by the nearest neighbors [83,84]), and the large fluctuations associated with collective motions in the quasistatic regime.

We observe that the average rotation rate $\langle\omega\rangle$ is simply related to the shear rate through the relation $\langle\omega\rangle = -\frac{1}{2}\dot{\gamma}$ [36]. This relation has been observed in other shear geometries (inclined plane flows, annular shear flows), in quasistatic deformations and with other discrete simulation methods [24,44,45,68,85]. Deviations are observed in the very first layers near the walls where the granular material is structured.

Consequently, $\dot{\gamma}$ is the natural scale of the rotation velocity, and from dimensional analysis, we analyze the variations of the dimensionless quantity $\delta\omega/\dot{\gamma}$ as a function of I. Since $\dot{\gamma}d$ is the natural scale of translation velocity, dimensional analysis suggests to analyze the variations of the dimensionless quantity $\delta v/\dot{\gamma}d$ as a function of I. Those variations, drawn in Fig. 10, evidence two scaling laws, independent of the parameters of the system:

$$\frac{\delta v}{\dot{\gamma}d} \simeq \frac{1}{3} I^{-\alpha},$$

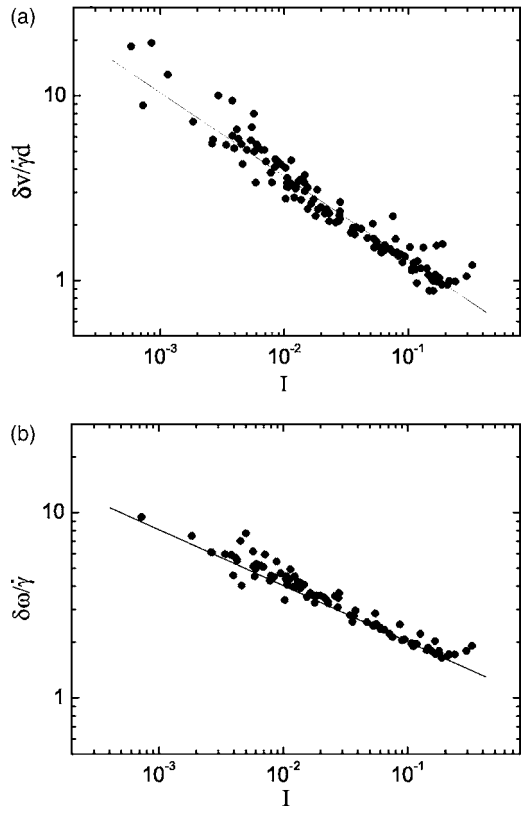

FIG. 10. Relative velocity fluctuations as a function of I: (a) translation velocity; (b) rotation velocity (various parameters).

$$\frac{\delta\omega}{\dot{\gamma}} \simeq I^{-\beta}, \tag{18}$$

with $\alpha \simeq \frac{1}{2}$ and $\beta \simeq \frac{1}{3}$, to which we shall refer as translation and rotation scaling laws.

The velocity fluctuations are significant (larger than 1) in the dense flow regime and very significant (larger than 10) in the quasistatic regime. In comparison, kinetic theory [see Eqs. (1) and (2)] predicts that $\delta v/\dot{\gamma}d = \sqrt{A_s/A_\Gamma}$ so that $\sqrt{(\pi+8)/32(1-e^2)} \simeq 1.3$, for $e=0.9$, which corresponds to the order of magnitude that is measured in the collisional regime.

Large values of $\delta\omega/\dot{\gamma}$ have been observed experimentally in the quasistatic regime [85] and in dense flows down inclined planes [45], and might be due to the frustration of the rotation [86].

We give two interpretations of the value of the exponent α. The first explanation [18] consists in analyzing the motion of one grain as a succession of shear phases of duration $1/\dot{\gamma}$ with a velocity $\dot{\gamma}d$ and of sudden rearrangements with a velocity $d\sqrt{P/m}$ of duration $\sqrt{m/P}$. This leads to $\delta v/\dot{\gamma}d \simeq I^{-1/2}(1-I)/(1+I)$. The second explanation relies on an energetic argument. In a steady uniform shear state, the work of the shear stress is balanced by the dissipation rate $S\dot{\gamma} = \Gamma$. If Γ describes the dissipation of the fluctuating kinetic energy $m\delta v^2/2$ during the inertial time $\sqrt{m/P}$, we obtain $\delta v/\dot{\gamma}d \simeq \sqrt{2\mu^*(I)}I^{-1/2}$. For both interpretations, the order of magnitude of the prefactor is consistent with the observation.

We now show that the translation scaling law is consistent with the variations of the relative fluctuations of the kinetic energy [Eq. (16)]. Let us call the average solid fraction of the granular materials $\rho=\rho_g\nu$ and the average kinetic energy by unit length $\langle E_c\rangle$. This is dominated by the translational part: $\langle E_c\rangle=(\rho/2)\int_0^H(\dot{\gamma}y)^2dy\sim(\rho V^2H)$. In the quasistatic regime, where the system oscillates between two localized flows $\Delta E_c\sim(\rho V^2H)/2$, so that $\Delta E_c/\langle E_c\rangle\sim 1$. In the collisional regime, $\Delta E_c\simeq(\rho/2)\int_0^H\delta v^2dy$. Using the translation scaling law for this last quantity, we get $\Delta E_c\sim\rho V^2/(HI)$, so that $\Delta E_c/\langle E_c\rangle\sim 1/(H^2I)$. This is in agreement with the dependencies on I and H observed in Fig. 9.

Furthermore, the translation scaling law provides an estimation of the Reynolds contribution to the stress tensor [see Eq. (5)]: $\Sigma^f/\Sigma\simeq(2\nu/9\pi)I$. This shows that for $I\leqslant 0.1$, this contribution remains smaller than 1%, so that the contribution of the contact forces Σ^c remains dominant.

C. Consequences for the constitutive law

The translation scaling law may also be written

$$\frac{\delta v}{d}\simeq\frac{1}{3}\dot{\gamma}^{1/2}(P/m)^{1/4}. \tag{19}$$

Consequently, when the pressure is prescribed, the velocity fluctuations vary like $\dot{\gamma}^{1/2}$, instead of $\dot{\gamma}$. We notice that, in the annular shear geometry, the pressure is constant along the radial direction, and an exponent close to 1/2 has been measured experimentally [70,87].

If we introduce the velocity fluctuations in the constitutive law, as in the collisional regime [see Eq. (1)], we obtain

$$P\simeq\frac{9a}{\nu_{max}-\nu}m(\delta v/d)^2,$$

$$S\simeq\frac{3b\sqrt{a}(\nu^*-\nu)}{(\nu_{max}-\nu)^{3/2}}m(\delta v/d)\dot{\gamma}. \tag{20}$$

Within this formulation, we notice a stronger divergency of the viscosity near the maximum solid fraction, as in the model inspired by the glassy dynamics [71].

VIII. CONTACT NETWORK

We now measure information on the contact network. Its strongly heterogeneous character in both space and time has already been discussed in detail [20,25,26,29,30,36,39,44,68,88–90]: the contact time varies from the short collision time in the fully collisional regime to the much longer shear time in the quasistatic regime [34,91], while the distribution of the force intensity is very wide [89]. We shall focus on the following three quantities: coordination number, mobilization of friction, and anisotropy of the contact forces.

A. Coordination number

As was shown in Fig. 1, the contact network is very sensitive to the inertial number. A small dilation of the material (around 10%) is enough to observe a transition from a dense contact network to multiple, or even binary, collisions between grains. A quantitative indicator is the coordination number Z, which is the average number of contacts per grain. The variations of Z as a function of I are shown in Fig. 11. Z increases as I decreases, and tends toward a maximum value Z_{max} when $I\to 0$. A possible fit is

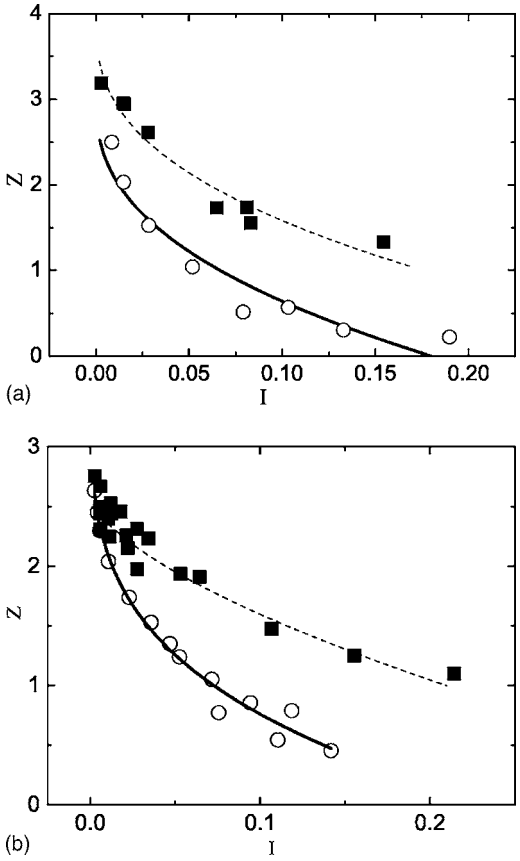

FIG. 11. Variation of the coordination number Z as a function of I [$\kappa=10^4$, $e=0.1$ (■) and 0.9 (○)]. (a) $\mu=0$: fits $Z=3.75-7.11I^{0.51}$ (−−), $Z=3.00-6.04I^{0.41}$ (−). (b) $\mu=0.4$: fits $Z=2.84-3.80I^{0.48}$ (−−), $Z=2.60-5.48I^{0.50}$ (−).

$$Z=Z_{max}-cI^{\gamma}, \tag{21}$$

which is drawn in Fig. 11, which gathers the results for a given contact stiffness number κ and various e and μ.

Figure 11 shows that the coordination number does not depend only on the geometry, through the solid fraction, but also on the mechanical properties of the grains e and μ. The exponent γ is nearly constant $\left(\gamma\simeq\frac{1}{2}\right)$, but Z_{max} and c depend on e and μ. When μ decreases, Z increases and Z_{max} tends to 4 for frictionless grains [92] [see Fig. 5(c)]. We also notice that Z increases when e decreases, due to the increasing collision time. Figure 12 indicates that Z_{max} decreases significantly with increasing κ, as expected.

B. Mobilization of friction

Inside the population of contacts, and for frictional grains, we introduce a distinction between the "sliding" contacts

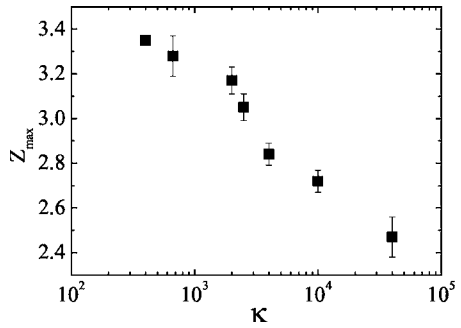

FIG. 12. Variation of the maximum coordination number as a function of κ ($e=0.1, \mu=0.4$).

where the local friction is completely mobilized ($|T|=\mu N$) and the other "rolling" contacts ($|T|\leqslant\mu N$). This distinction is different from the one proposed in [93] ("weak" and "strong" contacts), and a variant of the one proposed in [32], which distinguishes "fluid" contacts (collisions and sliding enduring contacts) and "solid" contacts (rolling enduring contacts). We define Z_s as the average number of sliding contacts per grain [94]. Figure 13(a) shows the variations of Z_s as a function of the inertial number I. We observe that Z_s increases with I in the quasistatic regime, up to a maximum in the dense flow regime. Moreover, Fig. 13(a) indicates that the $Z_s(I)$ curve depends on the restitution coefficient e.

We have shown on Fig. 13(b) the variations with I of the ratio $M=Z_s/Z$, which, as the proportion of sliding contacts,

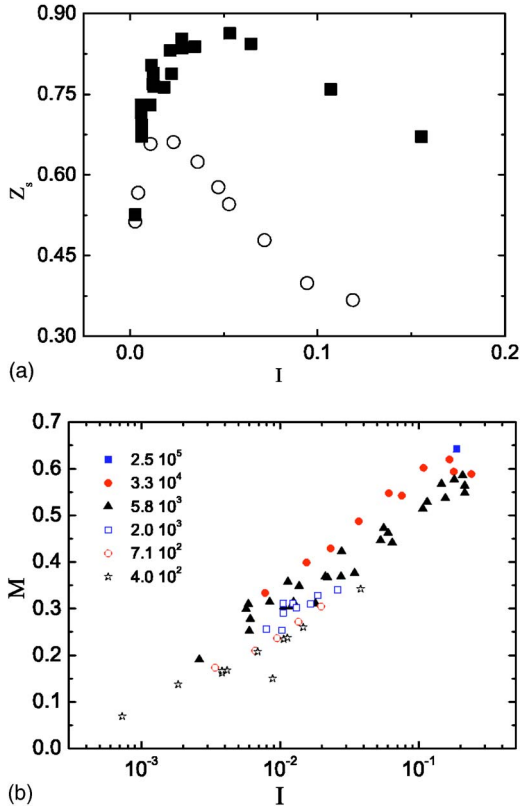

FIG. 13. (Color online) (a) Variation of Z_s as a function of I [$\mu=0.4$, $\kappa=4000$, $e=0.1$ (■) and 0.9 (○)]. (b) Variation of M as a function of I, for various κ.

is an indicator of the mobilization of friction. We observe that, contrarily to Z_s, M increases, approximately logarithmically, as a function of I. We also notice a slight increase of M when κ increases.

C. Anisotropy of the contact network

We now discuss the angular distribution of the contact network, whose importance in the quasistatic regime has been shown [9]. We call ϕ the direction of a contact counted counterclockwise from the x direction, between 0 and π. $(\vec{n}_\phi, \vec{t}_\phi)$ is the local frame in the direction ϕ. Let us call the average normal force in the homogeneous layer $\langle N\rangle$; then $\langle N(\phi)\rangle$ and $\langle T(\phi)\rangle$ are the average normal and tangential forces in the homogeneous layer in the direction ϕ. The anisotropies are described by the three angular distributions of contact orientations $\rho(\phi)$, of intensities of normal forces $\xi_N(\phi)=\langle N(\phi)\rangle/\langle N\rangle$ and of intensities of tangential forces $\xi_T(\phi)=\langle T(\phi)\rangle/\langle N\rangle$. Then we define $\zeta_N(\phi)=\rho(\phi)\xi_N(\phi)$ and $\zeta_T(\phi)=\rho(\phi)\xi_T(\phi)$. Those angular distributions satisfy the normalization relations

$$\int_0^\pi \rho(\phi)d\phi = 1,$$

$$\int_0^\pi \zeta_N(\phi)d\phi = 1,$$

$$\int_0^\pi \zeta_T(\phi)d\phi = 0. \tag{22}$$

We show in Fig. 14 the two quantities $\zeta_N(\phi)$ and $\zeta_T(\phi)$ which will be useful in the discussion of the friction law. We distinguish first quasistatic and collisional regimes, and second frictional and frictionless grains. A positive value of $\zeta_T(\phi)$ indicates that the tangential forces induce on average a counterclockwise rotation of the grains, and is represented with white symbols in Fig. 14(c). A negative value of $\zeta_T(\phi)$ indicates that the tangential forces induce on average a clockwise rotation of the grains, and is represented with black symbols in Fig. 14(c).

We notice a strong anisotropy of the contact network with privileged orientations for $\zeta_N(\phi)$ along the directions of shear ($\phi\simeq 0$ and π) and of maximum compression ($\phi\simeq 2\pi/3$), and for $\zeta_T(\phi)$ along the directions of shear ($\phi\simeq 0$ and π) and of the shear gradient ($\phi\simeq\pi/2$). Those anisotropies slightly change between the quasistatic and collisional regimes and between the frictional and frictionless grains cases.

Those anisotropies may be explained within a very simplified picture of a granular material organized in layers along the shear direction. Then, there are two kinds of contacts between grains, inside a layer ($\phi\simeq 0$ and π) and between layers ($\pi/3\leqslant\phi\leqslant 2\pi/3$). The contacts between layers are created along the direction of maximum compression ($\phi\simeq 2\pi/3$). In the quasistatic regime, those contacts are maintained up to the point where the grains separate (ϕ

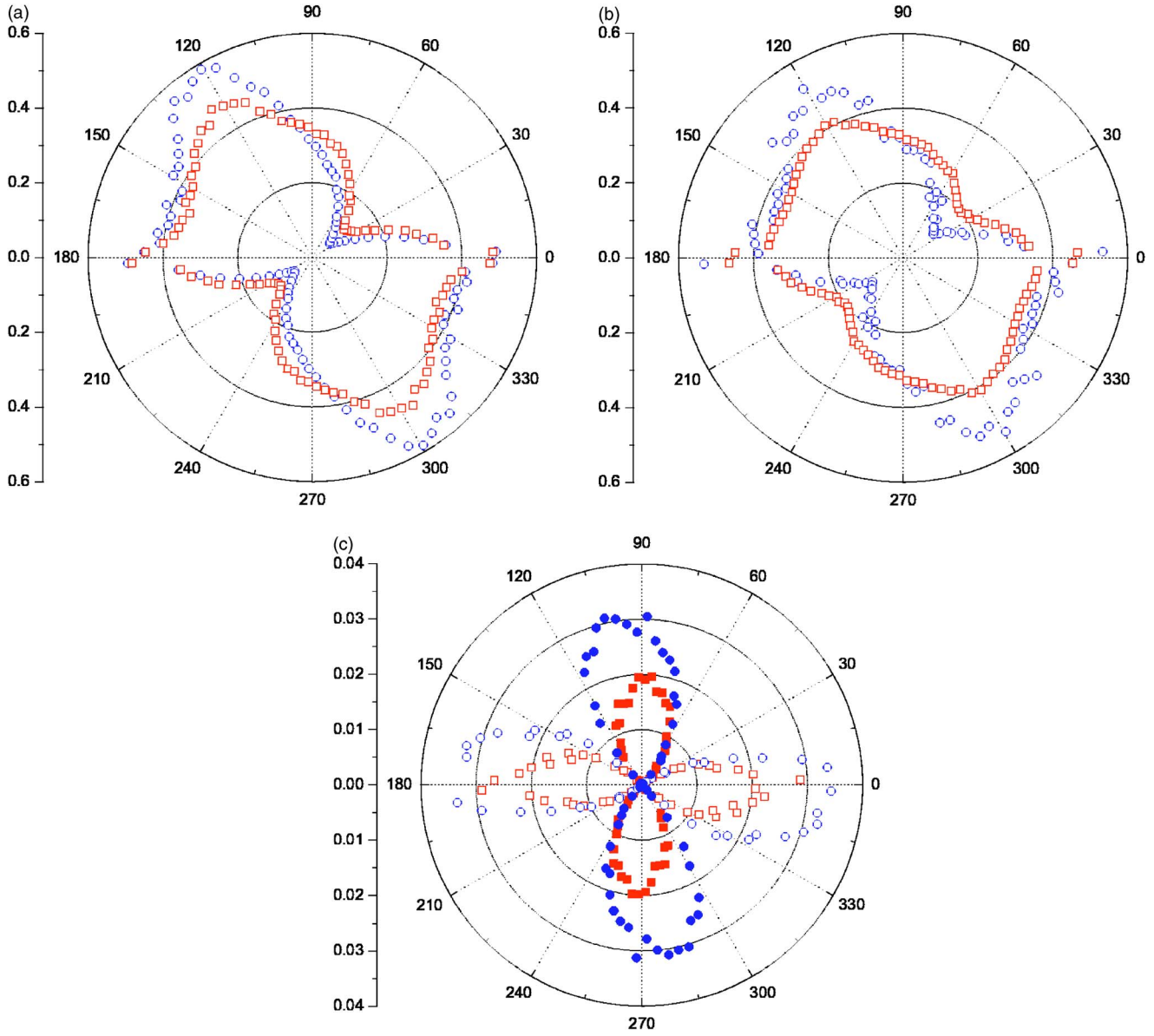

FIG. 14. (Color online) Angular distribution of the contact forces [quasistatic regime (I=0.005, □), collisional regime (I=0.13, ○): (a) $\zeta_N(\phi)$ (μ=0.4), (b) $\zeta_N(\phi)$ (μ=0), (c) $\zeta_T(\phi)$ (μ=0.4), ⩾0 white symbols, ⩽0 black symbols.

$\simeq \pi/3$). This is in contrast with the collisional regime where the grains bounce, so that ζ_N is stronger around $\pi/3$ and smaller between $\pi/3$ and $2\pi/3$.

We observe [see Fig. 15(a)] that the tangential anisotropy is well described by the following expression:

$$\zeta_T(\phi) = f_T(I)\zeta_N(\phi)\cos(2\phi), \tag{23}$$

with an increasing positive function $f_T(I)$. This means that contacts between layers favor a clockwise rotation of the grains, while contacts inside layers favor a counterclockwise rotation of the grains. Furthermore, this shows that the average tangential force is smaller in the quasistatic regime than in the collisional regime.

IX. MICROSCOPIC ORIGIN OF THE FRICTION LAW

We now try to understand quantitatively the effective friction law on the basis of microscopic information (fluctuations and anisotropy of the contact network). We refer to [55,77] for a similar attempt based on the analysis of the energy dissipation mechanisms, especially associated with the rotations of the grains.

A. Friction and rotation

We first discuss the tangential anisotropy and show how it is related to the rotation of the grains [86].

In a first step, we take into account the average rotation velocity ω. We consider the steady uniform shear of an assembly of grains of diameter d with an average shear rate $\dot{\gamma}$. Then, the tangential relative velocity between two grains is given by

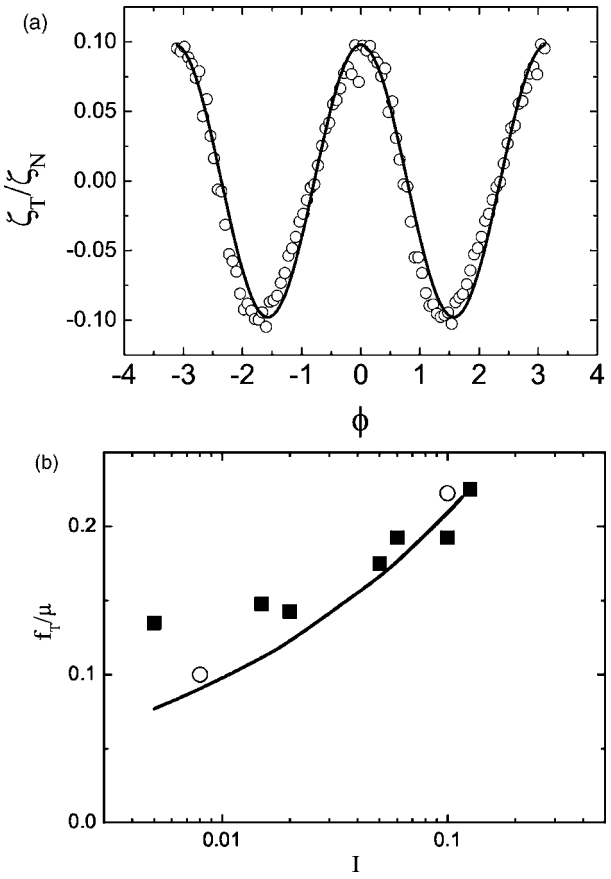

FIG. 15. Angular distribution of tangential contact forces: (a) $\zeta_T(\phi)/\zeta_N(\phi)$ (○) fitted by $f_T\cos(2\phi)$ (−) for $I=0.13$ and $\mu=0.4$; (b) $f_T(I)/\mu$ for $\mu=0.4$ (■) and 0.8 (○) compared with $(\sqrt{2}/\pi)I^{1/3}$.

$$V^T(\phi) = d[\omega + \dot{\gamma}\sin^2(\phi)]. \tag{24}$$

In steady state (no average torque exerted on the grain), the average tangential force exerted on a grain should be equal to zero:

$$\int_0^\pi \rho(\phi)T(\phi)d\phi = 0. \tag{25}$$

We start with two very crude assumptions: all the contacts are sliding $[T=-\mu N\,\mathrm{sgn}(V^T)]$ and the normal force distribution is isotropic $[\zeta_N(\phi)=1/\pi]$. Consequently,

$$\int_0^\pi \mathrm{sgn}[\omega + \dot{\gamma}\sin^2(\phi)]d\phi = 0. \tag{26}$$

This provides an explanation for the relation $\omega=-\frac{1}{2}\dot{\gamma}$, which was described in Sec. VII. Consequently $V^T(\phi)=-d\dot{\gamma}\cos(2\phi)/2$, $\zeta_T=\mu/\pi$ when $0\leqslant\phi\leqslant\pi/4$ and $3\pi/4\leqslant\phi\leqslant\pi$ and $\zeta_T=-\mu/\pi$ when $\pi/4\leqslant\phi\leqslant3\pi/4$. In comparison with Fig. 14(c), we notice that the sign of $\zeta_T(\phi)$ is correct, but that the order of magnitude is too large, by a factor of around 10.

As a way to understand the order of magnitude of $\zeta_T(\phi)$, we now take into account the fluctuations of the rotation velocity, which have been evidenced in Sec. VII. Denoting as $\delta\omega_{i,j}$ the fluctuations of rotation of two grains i and j in contact, their relative tangential velocity at the contact point becomes

$$V_{ij}^T(\phi) = -d\dot{\gamma}\cos(2\phi)/2 + d/2(\delta\omega_i + \delta\omega_j). \tag{27}$$

Keeping the assumption of sliding contacts, we predict

$$\zeta_T(\phi) = -\mu\zeta_N(\phi)\langle\mathrm{sgn}(V^T)\rangle, \tag{28}$$

where $\langle\mathrm{sgn}(V^T)\rangle$ is the statistical average over the fluctuating rotations of the two grains. Discrete numerical simulations have shown that the distribution of the rotation velocity is approximately Lorentzian [45]. We make the assumption that the fluctuations of rotation of two grains in contact are not correlated. Then the random variable $(\delta\omega_i+\delta\omega_j)/2$ follows a Lorentzian distribution, with a zero mean value and a variance $\delta\omega/\sqrt{2}$. Then we obtain

$$\langle\mathrm{sgn}(V^T)\rangle = -\frac{2}{\pi}\arctan\left(\frac{\dot{\gamma}}{\sqrt{2}\delta\omega}\cos(2\phi)\right). \tag{29}$$

Using the rotation scaling law (18),

$$\langle\mathrm{sgn}(V^T)\rangle = -\frac{2}{\pi}\arctan\left(\frac{I^{1/3}}{\sqrt{2}}\cos(2\phi)\right), \tag{30}$$

and for small I ($\leqslant 0.2$)

$$\langle\mathrm{sgn}(V^T)\rangle \simeq -\frac{\sqrt{2}}{\pi}I^{1/3}\cos(2\phi), \tag{31}$$

so that finally

$$\zeta_T(\phi) \simeq \frac{\sqrt{2}}{\pi}\mu I^{1/3}\zeta_N(\phi)\cos(2\phi). \tag{32}$$

This expression reproduces the observed angular dependence in $\zeta_N(\phi)\cos(2\phi)$, shown in Fig. 15(a). The prediction for the dependence of the amplitude on I and μ is in agreement with the observed prefactor $f_T(I)$ defined in Eq. (23), as shown in Fig. 15(b). The order of magnitude is now consistent with the observations.

As a conclusion, the fluctuations of the rotation velocity are a possible quantitative explanation of the angular distribution of tangential forces $\zeta_T(\phi)$. When I decreases, the relative fluctuations of rotation increase, so that the average relative tangential velocity of two grains in contact tends to zero, which kills the frictional effect. This model is very crude. In the collisional regime, we have seen that most of the contacts are sliding (see Fig. 13) and the assumption of uncorrelated fluctuations may seem reasonable. On the contrary, in the quasistatic regime, we have observed that most of the contacts are rolling. Furthermore, our simulations reveal correlations of the rotations of grains in contact: it seems that the flowing granular material is organized in clusters of grains rotating in the same way [86]. Such correlations of the grain motion deserve further study [56,95].

B. Friction and anisotropy

We now discuss the friction law $\mu^*(I)$ on the basis of the information on the contact network. We would like to under-

stand the increase of μ^* with I, and its dependence with the microscopic friction μ.

A first possible interpretation lies in the increase of the mobilization of friction $M(I)$ [Fig. 13(b)]: most of the contacts are rolling in the quasistatic regime, while most of them are dissipative sliding collisions in the collisional regime. Consequently, the energy dissipation, and hence the effective friction, should be stronger in the collisional regime. However, since the effective friction coefficient of an assembly of frictionless grains is not equal to zero, this interpretation is certainly not sufficient. We are now going to show the crucial role of the anisotropies of the contact network.

We consider the steady uniform shear of an assembly of grains of diameter d with average solid fraction ν, coordination number Z, and normal force $\langle N \rangle$. The stress tensor is dominated by the contribution of the contacts [see Eq. (5)]. It is possible to express it as a function of the angular distributions of contact forces, which we have previously defined [45,85,96,97]:

$$\underline{\underline{\Sigma}} = \frac{2\nu Z\langle N\rangle}{\pi d}\int_0^{\pi} [\zeta_N(\phi)\vec{n}_\phi - \zeta_T(\phi)\vec{t}_\phi] \otimes \vec{n}_\phi d\phi. \quad (33)$$

Using the properties of the stress tensor ($\Sigma_{xy}=\Sigma_{yx}$ and $\Sigma_{xx}=\Sigma_{yy}$) and the normalization of angular distributions [Eqs. (22)], the effective friction coefficient takes the simple expression:

$$\mu^* = -\int_0^{\pi} [\zeta_N(\phi)\sin(2\phi) - \zeta_T(\phi)\cos(2\phi)]d\phi. \quad (34)$$

In the first term associated with the normal forces (μ_N^*), the factor $\sin(2\phi)$ is positive for ϕ between 0 and $\pi/2$, so that it decreases the effective friction, and negative for ϕ between $\pi/2$ and π, so that it increases the effective friction. Consequently, the evolution of the angular distribution between the quasi-static regime and the collisional regime [see Figs. 14(a) and 14(b)] might explain part of the increase of the effective friction.

It is possible to give an estimation of the second term associated with the tangential forces (μ_T^*), using the approximation (32) for $\zeta_T(\phi)$, with $\zeta_N(\phi)=1/\pi$. We obtain $\mu_T^* \simeq (\mu/\sqrt{2}\pi)I^{1/3}$. This contribution is small. The complete calculation [Fig. 16(b)] confirms that the contribution of tangential forces to the effective friction ($|\mu_T^*|/\mu*$) remains of the order of 12% for $\mu=0.4$ and 18% for $\mu=0.8$. A similar conclusion was drawn by [55] from an assumption of isotropic contact force distribution.

Figure 16(a) compares the prediction based on the angular distribution (34) with the complete calculation based on (5), for both frictional and frictionless grains (the results of Fig. 6). The agreement is excellent.

The friction law depends mostly on the angular distribution of normal forces. When going from the quasistatic to the collisional regime, the small increase of the anisotropy increases the effective friction coefficient by a factor of two. In the same way, the decrease of the friction law when going from frictional to frictionless grains is due to a more isotropic angular distribution of normal forces. The microscopic friction coefficient has an indirect effect on the friction law, through the modification of the angular distribution of normal forces. This would mean that the very origin of the viscoplastic constitutive law relies on the anisotropy of the contact network in response to the shear. This point, which has already been studied in the quasistatic regime [9], deserves further study.

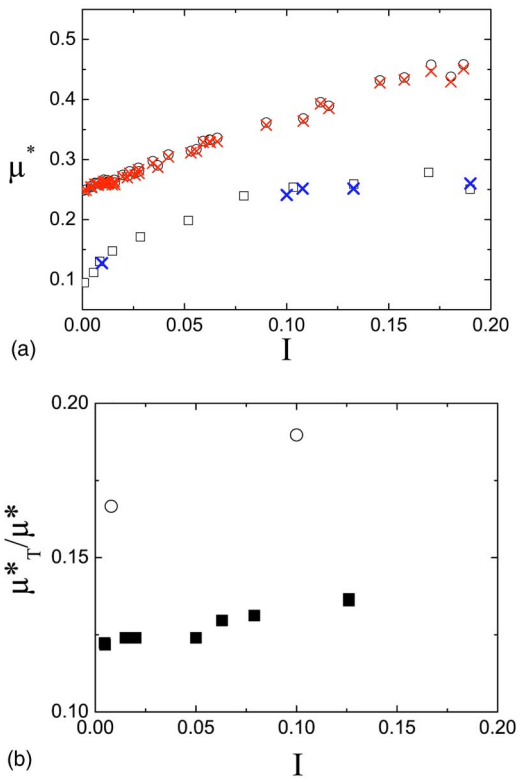

FIG. 16. (Color online) Friction and anisotropy. (a) Comparison of Eq. (34) (cross) with direct measurement of Fig. 6 (open symbols) [$\mu=0$ (□), $\mu=0.4$ (○)]. (b) Tangential contribution for $\mu=0.4$ (■) and 0.8 (○).

X. CONCLUSION

We now summarize our conclusions. We have considered the simplest flow geometry (plane shear without gravity), where the stress distribution is uniform. Using molecular dynamics simulation, we have submitted a dense assembly of dissipative disks to a given pressure and shear rate. We have observed steady uniform shear flows, which become intermittent in the quasistatic regime. We have shown that, in the limit of rigid grains, the shear state is determined by a single dimensionless number, called the inertial number I, which describes the ratio of inertial to pressure forces. Small values of I correspond to the quasistatic critical state regime of soil mechanics, while large values of I correspond to the fully collisional regime of kinetic theory. When I increases in the dense flow regime, we have measured an approximately linear decrease of the solid fraction from the maximum packing value, and an approximately linear increase of the effective friction coefficient from the static internal friction value. From those dilatancy and friction laws, we have deduced a

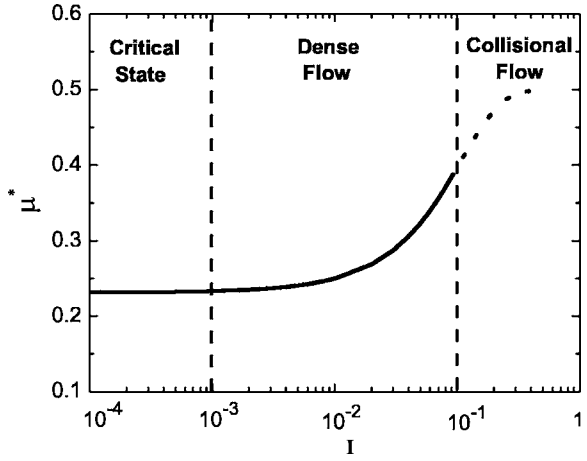

FIG. 17. Diagram of the granular flow regimes.

viscoplastic constitutive law, with a plastic Coulomb term and a viscous Bagnold term. We have shown that this constitutive law is not very sensitive to the mechanical properties of the grains, once they are frictional, dissipative, and rigid. We have measured the evolution of the relative velocity fluctuations and of the contact force anisotropy as a function of I. Based on those microstructural information, we have proposed a simple explanation of the friction law.

Figure 17 shows a qualitative diagram of the flow regimes and of the friction law. The quasistatic critical state regime corresponds to very small values of I, with nearly no variation of the effective friction coefficient. The transition between the quasistatic regime and the dense flow regime is not very well defined. It may correspond to the transition between intermittent and continuous flow regime, for $I \simeq 10^{-3}$, which may depend on the system size [18,36]. The transition between the dense flow regime and the fully collisional flow regime occurs for $I \simeq 10^{-1}$. The effective friction coefficient increases in the dense flow regime and should saturate in the fully collisional regime (the values of the effective friction coefficient in the figure are indicative).

Other simulations of steady uniform shear states without walls have confirmed those observations [98]. A generalization of our results to other flow geometries (annular shear, vertical chute, inclined plane, heap flows) is discussed in [18,36]. Then, even if the same qualitative tendencies are observed, it seems that other dimensionless quantities (associated with gravity, proximity of the wall, stress gradients, etc.) should be introduced. We notice that a generalization of those ideas to steady uniform shear flows of cohesive granular materials has been successful [98]. In this paper, we have restricted our attention to velocity controlled shear flows, so that it was not possible to study the flow threshold (evidenced indirectly through the appearance of intermittencies for small enough I [56]). A specific study of the jamming mechanisms should be performed by controlling the shear stress, either in plane shear flows [32] or down inclined planes [36,67].

ACKNOWLEDGMENTS

We gratefully acknowledge Lydéric Bocquet, Philippe Coussot, Ivan Iordanoff, Jim Jenkins, Pierre Mills, and Olivier Pouliquen for many interesting discussions at various stages of this study. Laboratoire des Matériaux et Structures du Génie Civil is a joint laboratory, depending on Laboratoire Central des Ponts et Chaussées, Ecole Nationale des Ponts et Chaussées and Centre National de la Recherche Scientifique.

[1] K. R. Hutter and K. R. Rajagopal, Continuum Mech. Thermodyn. **6**, 81 (1994).
[2] J. Rajchenbach, Adv. Phys. **49**, 229 (2000).
[3] *The Physics of Granular Media*, edited by H. Hinrichsen and D. Wolf (Wiley-VCH, Weinheim, 2004).
[4] R. Jackson, in *Theory of Dispersed Multiphase Flow*, edited by R. Meyer (Academic Press, New York, 1983), pp. 291–337.
[5] R. Nedderman, *Statics and Kinematics of Granular Materials* (Cambridge University Press, Cambridge, U.K., 1992).
[6] G. Tardos, Powder Technol. **92**, 61 (1997).
[7] P. A. Vermeer, in *Physics of Dry Granular Media*, edited by H. J. Hermann, J. P. Hovi, and S. Luding (Balkema, Dordrecht, 1998), pp. 163–196.
[8] D. M. Wood, *Soil Behaviour and Critical State Soil Mechanics* (Cambridge University Press, Cambridge, U.K., 1990).
[9] F. Radjai and S. Roux, in *The Physics of Granular Media* (Ref. [3]), pp. 165–187.
[10] P. K. Haff, J. Fluid Mech. **134**, 401 (1983).
[11] J. T. Jenkins and S. B. Savage, J. Fluid Mech. **130**, 187 (1983).
[12] J. T. Jenkins and M. W. Richman, Phys. Fluids **28**, 3485 (1985).
[13] C. S. Campbell, Annu. Rev. Fluid Mech. **22**, 57 (1990).
[14] I. Goldhirsch, Annu. Rev. Fluid Mech. **35**, 267 (2003).
[15] S. Luding, Phys. Rev. E **63**, 042201 (2001).
[16] F. Radjai and S. Roux, Phys. Rev. Lett. **89**, 064302 (2002).
[17] O. Pouliquen and F. Chevoir, C. R. Phys. **3**, 163 (2002).
[18] G. D. R. Midi, Eur. Phys. J. E **14**, 341 (2004).
[19] P. A. Cundall, Ing.-Arch. **59**, 148 (1989).
[20] M. Babic, H. H. Shen, and H. T. Shen, J. Fluid Mech. **219**, 81 (1990).
[21] P. A. Thompson and G. S. Grest, Phys. Rev. Lett. **67**, 1751 (1991).
[22] Y. Zhang and C. S. Campbell, J. Fluid Mech. **237**, 541 (1992).
[23] J. D. Dent, Ann. Glaciol. **18**, 215 (1993).
[24] C. K. K. Lun and A. A. Bent, J. Fluid Mech. **258**, 335 (1994).
[25] O. J. Schwarz, Y. Horie, and M. Shearer, Phys. Rev. E **57**, 2053 (1998).
[26] E. Aharonov and D. Sparks, Phys. Rev. E **60**, 6890 (1999).
[27] J. K. Morgan, J. Geophys. Res. **104**, 2721 (1999).
[28] H. Hayakawa, Prog. Theor. Phys. Suppl. **138**, 537 (2000).
[29] P. Jalali, W. Polashenski, T. Tynjälä, and P. Zamankhan, Physica D **162**, 188 (2002).
[30] E. Aharonov and D. Sparks, Phys. Rev. E **65**, 051302 (2002).

[31] C. S. Campbell, J. Fluid Mech. **465**, 261 (2002).
[32] D. Volfson, L. S. Tsimring, and I. Aranson, Phys. Rev. E **68**, 021301 (2003).
[33] I. Iordanoff and M. M. Khonsari, J. Tribol. **126**, 137 (2004).
[34] H. H. Shen and B. Sankaran, Phys. Rev. E **70**, 051308 (2004).
[35] G. Lois, A. Lemaitre, and J. M. Carlson, e-print cond-mat/0501535.
[36] F. da Cruz, Ph.D. thesis, Ecole Nationale des Ponts et Chaussées, 2004, http://pastel paristech.org/archive/00000946.
[37] K. L. Johnson, *Contact Mechanics* (Cambridge University Press, Cambridge, U.K., 1985).
[38] N. Brilliantov, F. Spahn, J. M. Hertzsch, and T. Pöschel, Phys. Rev. E **53**, 5382 (1996).
[39] S. Schollmann, Phys. Rev. E **59**, 889 (1999).
[40] P. A. Cundall and O. D. L. Strack, Geotechnique **29**, 47 (1979).
[41] L. E. Silbert, D. Ertas, G. S. Grest, T. C. Halsey, D. Levine, and S. J. Plimpton, Phys. Rev. E **64**, 051302 (2001).
[42] J.-N. Roux and F. Chevoir, Bull. Lab. Ponts Chaussees **254**, 109 (2005).
[43] M. P. Allen and D. J. Tildesley, *Computer Simulation of Liquids* (Oxford University Press, Oxford, 1987).
[44] M. Lätzel, S. Luding, and H. J. Hermann, Granular Matter **2**, 123 (2000).
[45] M. Prochnow, Ph.D. thesis, Ecole Nationale des Ponts et Chaussées, 2002, http://pastel.paristech.org/archive/00000321
[46] O. R. Walton and R. L. Braun, J. Rheol. **30**, 949 (1986).
[47] J. P. Hansen and I. R. McDonald, *Theory of Simple Liquids* (Academic Press, London, 1986).
[48] J. Christoffersen, M. M. Mehrabadi, and S. Nemat-Nasser, J. Appl. Mech. **48**, 339 (1981).
[49] N. Kruyt and L. Rothenburg, J. Appl. Mech. **118**, 706 (1996).
[50] J.-J. Moreau, in *Friction, Arching, Contact Dynamics*, edited by D. E. Wolf and P. Grassberger (World Scientific, London, 1997), pp. 233–247.
[51] C. Thornton and L. Zhang, Philos. Mag. (to be published).
[52] F. da Cruz, F. Chevoir, J. N. Roux, and I. Iordanoff, in *Transient Processes in Tribology*, edited by G. Dalmaz, A. A. Lubrecht, D. Dowson, and M. Priest (Elsevier, Amsterdam, 2004).
[53] J. N. Roux and G. Combe, C. R. Phys. **3**, 131 (2002).
[54] S. B. Savage and K. Hutter, J. Fluid Mech. **199**, 177 (1989).
[55] C. Ancey, P. Coussot, and P. Evesque, J. Rheol. **43**, 1673 (1999).
[56] P. Mills, P. G. Rognon, and F. Chevoir, in *Powders and Grains* 2005, edited by R. Garcia-Rojo, H. J. Herrmann, and S. McNamara, (A.A. Balkiema Publishers, Leiden, The Netherlands, 2005), pp. 365-368.
[57] C. Goujon, N. Thomas, and B. Dalloz-Dubrujeaud, Eur. Phys. J. E **11**, 147 (2003).
[58] G. Chambon, J. Schmittbuhl, A. Corfdir, J.-P. Vilotte, and S. Roux, Phys. Rev. E **68**, 011304 (2003).
[59] G. Ovarlez and E. Clément, Phys. Rev. E **68**, 031302 (2003).
[60] S. B. Savage and M. Sayed, J. Fluid Mech. **142**, 391 (1984).
[61] M. Hanes and D. Inman, J. Geophys. Res. **90**, 3670 (1985).
[62] K. Craig, R. H. Buckholz, and G. Domoto, J. Appl. Mech. **53**, 935 (1986).
[63] C. S. Campbell, P. W. Cleary, and M. Hopkins, J. Geophys. Res. **100**, 8267 (1995).
[64] A. V. Potapov and C. S. Campbell, Phys. Fluids **8**, 2884 (1996).
[65] O. Pouliquen, Phys. Fluids **11**, 542 (1999).
[66] O. Pouliquen and Y. Forterre, J. Fluid Mech. **453**, 133 (2002).
[67] F. da Cruz, M. Prochnow, J.-N. Roux, and F. Chevoir, in *Powders and Grains* 2005, Ref. [56], pp. 361-364.
[68] D. Howell, R. Behringer, and C. Veje, Chaos **9**, 559 (1999).
[69] R. A. Bagnold, Proc. R. Soc. London, Ser. A **225**, 49 (1954).
[70] L. Bocquet, W. Losert, D. Schalk, T. C. Lubensky, and J. P. Gollub, Phys. Rev. E **65**, 011307 (2002).
[71] L. Bocquet, J. Errami, and T. C. Lubensky, Phys. Rev. Lett. **89**, 184301 (2002).
[72] C. Josserand, P.-Y. Lagree, and D. Lhuillier, Eur. Phys. J. E **14**, 127 (2004).
[73] P. C. Johnson and R. Jackson, J. Fluid Mech. **176**, 67 (1987).
[74] L. S. Mohan, P. R. Nott, and K. K. Rao, Chem. Eng. Sci. **52**, 913 (1997).
[75] S. B. Savage, J. Fluid Mech. **377**, 1 (1998).
[76] P. Mills, D. Loggia, and M. Tixier, Europhys. Lett. **45**, 733 (1999).
[77] C. Ancey, Phys. Rev. E **62**, 8349 (2000).
[78] J. Rajchenbach, Eur. Phys. J. E **14**, 367 (2004).
[79] D. M. Hanes, J. T. Jenkins, and M. W. Richman, J. Appl. Mech. **55**, 969 (1988).
[80] S. Nasuno, A. Kudrolli, A. Bak, and J. P. Gollub, Phys. Rev. E **58**, 2161 (1998).
[81] M. Lubert and A. de Ryck, Phys. Rev. E **63**, 021502 (2001).
[82] F. da Cruz, F. Chevoir, D. Bonn, and P. Coussot, Phys. Rev. E **66**, 051305 (2002).
[83] O. Pouliquen, M. Belzons, and M. Nicolas, Phys. Rev. Lett. **91**, 014301 (2003).
[84] G. Marty and O. Dauchot, Phys. Rev. Lett. **94**, 015701 (2005).
[85] F. Calvetti, G. Combe, and J. Lanier, Mech. Cohesive-Frict. Mater. **2**, 121 (1997).
[86] M. R. Kuhn and K. Bagi, J. Eng. Mech. **130**, 826 (2004).
[87] D. Mueth, Phys. Rev. E **67**, 011304 (2003).
[88] C. Denniston and H. Li, Phys. Rev. E **59**, 3289 (1999).
[89] F. Radjai, in *Powders and Grains*, edited by Y. Kishino (Lisse, Swets and Zeitlinger, Sendai, Japan, 2001), pp. 157–160.
[90] C. O'Hern, S. A. Langer, A. J. Liu, and S. R. Nagel, Phys. Rev. Lett. **86**, 111 (2001).
[91] D. Z. Zhang and A. Rauenzahn, J. Rheol. **44**, 1019 (2000).
[92] J.-N. Roux, Phys. Rev. E **61**, 6802 (2000).
[93] F. Radjai, D. Wolf, M. Jean, and J. Moreau, Phys. Rev. Lett. **80**, 61 (1998).
[94] L. Staron, J.-P. Vilotte, and F. Radjai, Phys. Rev. Lett. **89**, 204302 (2002).
[95] O. Pouliquen, Phys. Rev. Lett. **93**, 248001 (2004).
[96] K. I. Kanatani, Powder Technol. **28**, 167 (1981).
[97] B. Cambou, P. Dubujet, F. Emeriault, and F. Sidoroff, Eur. J. Mech. A/Solids **14**, 255 (1995).
[98] P. G. Rognon, M. Naaim, J. N. Roux, and F. Chevoir, in *Powders and Grains* 2005, Ref. [56] pp.565-568.